Virtual Axle Method for Bridge Weigh-in-Motion Systems Requiring No Axle Detector

Article *in* Journal of Bridge Engineering · September 2019

DOI: 10.1061/(ASCE)BE.1943-5592.0001474

4 authors:

Wei He
Hunan University

Tianyang Ling
Hunan University

Eugene J. OBrien
University College Dublin

Lu Deng
Hunan University

Virtual Axle Method for Bridge Weigh-in-Motion Systems Requiring No Axle Detector

Wei He[1]; Tianyang Ling[2]; Eugene J. OBrien[3]; and Lu Deng, Ph.D., M.ASCE[4]

Abstract: Bridge weigh-in-motion (BWIM) systems provide an effective approach to identifying the axle and gross vehicle weights of vehicles as they travel over an instrumented bridge. For the majority of BWIM systems, the vehicle configuration (including axle count and axle spacing) and vehicle speed are prerequisites for identifying the axle and gross weights of vehicles. Existing nothing-on-road (NOR) BWIM systems acquire such data through dedicated sensors, namely, free-of-axle-detector (FAD) sensors, in addition to weighing sensors. These FAD sensors are usually installed on the underside of the bridge deck or girders. This study presents a novel method for identifying the axle spacing and weights of vehicles. It only requires the flexural strain signal recorded from the weighing sensors, leading to both a reduction in the installation cost and broader applications of BWIM systems. The effectiveness and accuracy of the proposed method are demonstrated through numerical simulations. Laboratory experiments based on a scaled vehicle–bridge interaction (VBI) model were also conducted for verification. The results show that the proposed method has good accuracy for axle spacing and axle weight identification. **DOI: 10.1061/(ASCE)BE.1943-5592.0001474.**

Author keywords: Bridge weigh-in-motion (BWIM); Strain; Axle spacing; Vehicle weight; Overload.

Introduction

Accurate traffic load information is of great value for the assessment and maintenance of transportation infrastructure (Deng et al. 2017, 2018a). Traffic monitoring, especially of vehicle weights, is of significance for traffic management and load-limit enforcement (Jacob 2010; Richardson et al. 2014). Bridge weigh-in-motion (BWIM) is one of many technologies used today for weighing vehicles as they travel at highway speed. The concept, which was first proposed by Moses in the 1970s (Moses 1979), uses an instrumented bridge as a scale to weigh the vehicles passing over bridges at normal speeds. Over the years, Moses's algorithm has been the basis for many other schemes aiming to improve the accuracy and applicability of BWIM systems (Quilligan et al. 2002; Richardson et al. 2014; Sekiya et al. 2018; Yu et al. 2018; Zhao et al. 2014). State-of-the-art reviews on BWIM algorithms and their applications have been presented by Yu et al. (2016) and Lydon et al. (2016).

Moses's algorithm and its variants generally estimate the axle weights of vehicles by minimizing the Euclidean norm of the residual between the actual bridge response measured from weighing sensors and the predicted bridge response based on the influence line method. The axle information (i.e., the number of axles and axle spacing) and vehicle speed are prerequisites for predicting bridge responses. Axle detectors have therefore been developed for this purpose and are needed for the majority of existing BWIM systems. Conventional axle detectors identify vehicle axles using pressure-sensitive sensors installed on the upper surface of the bridge deck. This method is quite simple and has good accuracy. However, the sensors are directly exposed to the impact of wheels and are therefore not durable. In addition, the installation raises issues of safety and may cause disruption to traffic. To address this issue, nothing-on-road (NOR) BWIM systems and free-of-axle-detector (FAD) systems have been proposed (OBrien and Žnidarič 2001). In the FAD scheme, vehicle axles are detected from the local response measured by special sensors attached underneath the bridge deck. However, the FAD scheme is suitable only for specific types of bridges and is sensitive to the deck thickness, surface roughness, and vehicle transverse position (Ieng et al. 2012; Kalin 2006; OBrien and Žnidarič 2001).

To overcome the disadvantages of conventional FAD methods, some researchers have attempted to use the global flexural strain information acquired from the weighing sensors to identify the vehicle speed and axle spacing. Wall et al. (2009) obtained the vehicle velocity and axle configuration by calculating the second derivative of the bending responses of the bridge. Kalhori et al. (2017) found that vehicle axles can be identified by applying a peak analysis to the time history of flexural strains, although some axles might occasionally become unidentifiable. Yu et al. (2015) proposed a vehicle axle identification method using only the global strain signal from the weighing sensors based on a wavelet transformation. A shear-force-based method was recently shown to be an effective and efficient method for axle identification (OBrien et al. 2012), whereas Lydon et al. (2017) used bearing strain with axle detection with good success. Bao et al. (2016), based on field test results, found that vehicle weights could also be estimated from measured shear strains. In addition to these methods, a novel virtual simply-supported beam (VSSB) method was proposed by He et al. (2016), which identifies vehicle axles based on the flexural bending strains measured from four different longitudinal positions of the bridge

[1]Research Assistant, College of Civil Engineering, Hunan Univ., Changsha, Hunan 410082, China. Email: hewei.hnu@gmail.com

[2]Research Assistant, College of Civil Engineering, Hunan Univ., Changsha, Hunan 410082, China. Email: lingtianyang@126.com

[3]Professor, School of Civil Engineering, Univ. College Dublin, Dublin D04V1W8, Ireland. ORCID: https://orcid.org/0000-0002-6867-1009. Email: eugene.obrien@ucd.ie

[4]Professor, Key Laboratory for Damage Diagnosis of Engineering Structures of Hunan Province, Hunan Univ., Changsha, Hunan 410082, China (corresponding author). Email: denglu@hnu.edu.cn

Note. This manuscript was submitted on January 22, 2019; approved on May 2, 2019; published online on June 24, 2019. Discussion period open until November 24, 2019; separate discussions must be submitted for individual papers. This paper is part of the ***Journal of Bridge Engineering***, © ASCE, ISSN 1084-0702.

girder. Furthermore, an advanced equivalent shear force (ESF) method was proposed (Deng et al. 2018b), which reduces the number of measurement sections needed to three. Compared to other methods, these two approaches do not require complicated signal analysis and are not restricted to certain bridge types or boundary conditions. However, all these methods require additional sensors besides the weighing sensors.

Additionally, some new types of sensors and devices have been adopted for BWIM systems. Lydon et al. (2017) proposed the use of fiber-optic sensors monitoring bearing strains for axle detection in their NOR BWIM system. Ojio et al. (2016) proposed a vision-system-based contactless BWIM system that uses roadside cameras to detect vehicle speed and axle spacing. These methods showed good potential in some aspects for future BWIM systems.

In this study, a novel virtual axle (VA) method is proposed to identify vehicle axle spacing and axle weight. This method uses precalibrated bridge influence lines, measured bridge responses, and preacquired vehicle speed in the identification process. Compared with existing NOR systems, this method requires no additional devices or sensors for axle detection during the weighing procedure. Numerical simulations and laboratory experiments were conducted to validate the effectiveness and accuracy of the proposed VA method.

Theory

Moses's Algorithm

The fundamental basis of most BWIM systems is Moses's algorithm. Typically, for an instrumented girder bridge, the total flexural bending moment at a specific cross section can be obtained by the following expression:

$$M_k = \sum_{i}^{m} ES_i \varepsilon_{i,k} \tag{1}$$

where $\varepsilon_{i,k}$ = measured bending strain from the kth scan at the ith lateral position at a specific cross section; m = number of measurement points (lateral positions) at the cross section; E = Young's modulus of the bridge girder; and S_i = section modulus related to the ith girder (and associated slab, if applicable) at the measurement section.

The total flexural bending moment can also be determined theoretically from the following equation:

$$M_k^{\mathrm{T}} = \sum_{j=1}^{N} I(v \cdot t_k - x_j) \cdot P_j \tag{2}$$

where N = number of vehicle axles; $I(x)$ = influence line function value at the loading position x; v = vehicle speed; t_k = time corresponding to the kth scan; x_j = position of the jth axle relative to the first; and P_j = jth axle load. For a total of K scans and N axles, Eq. (2) can be expressed in matrix form as

$$\mathbf{M}' = \begin{Bmatrix} M'_1 \\ M'_2 \\ \vdots \\ M'_K \end{Bmatrix} = \mathbf{I} \cdot \mathbf{P} = \begin{bmatrix} I_{1,1} & I_{1,2} & \cdots & I_{1,N} \\ I_{2,1} & I_{2,2} & & \\ \vdots & & \ddots & \\ I_{K,1} & & & I_{K,N} \end{bmatrix} \begin{Bmatrix} P_1 \\ P_2 \\ \vdots \\ P_N \end{Bmatrix} \tag{3}$$

where $I_{j,k} = I(v \cdot t_k - x_j)$ is the influence ordinate corresponding to the position of the jth axle at time t_k.

The determination of axle loads $\mathbf{P}$ can be addressed by solving a linear least-squares problem (i.e., finding a vector to minimize E, the Euclidean norm of residual $\mathbf{M} - \mathbf{M}'$), which can be expressed as follows:

$$E = \|\mathbf{M} - \mathbf{M}'\|_2^2 = \sum_{k=1}^{K} (M_k - M'_k)^2 \tag{4}$$

The axle load vector $\mathbf{P}$ is given by

$$\mathbf{P} = (\mathbf{I}^T \mathbf{I})^{-1} \mathbf{I} \cdot \mathbf{M} \tag{5}$$

where the superscript T indicates the matrix transpose.

Virtual Axle Method

In the method proposed in this study, a vehicle is assumed to have a large number of VAs that are evenly distributed in the longitudinal direction and can cover the whole range of the wheelbase. All axles other than the true ones are assumed to have zero weight. Then, the goal of the proposed method is to identify the true axles and their weights.

A three-axle example truck is used to illustrate the concept. This truck has weights of 50, 200, and 150 kN for Axles 1–3, respectively, and the axle spacings are 5 and 3 m, as illustrated in Fig. 1. Assuming that the truck passes over a 20-m simply-supported bridge, the bending moment at the center can be calculated, as presented in Fig. 2, where the solid curve is the moment due to the whole vehicle, whereas the dashed and dotted curves are the bending moments due to each of the three axles.

It is first assumed that the truck has a large number of evenly spaced VAs at axle spacings of 0.05 m, along a length of 12 m in the longitudinal direction starting from +2 m and extending back to −10 m relative to the position of the first real axle (Fig. 1). For this example, there is a total of 241 VAs (of which three coincide with the real axle locations). The 12-m length is so selected to cover all three true axle locations in the longitudinal direction, and the

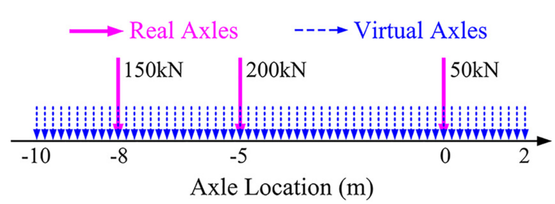

Fig. 1. Real and virtual axles of a three-axle truck.

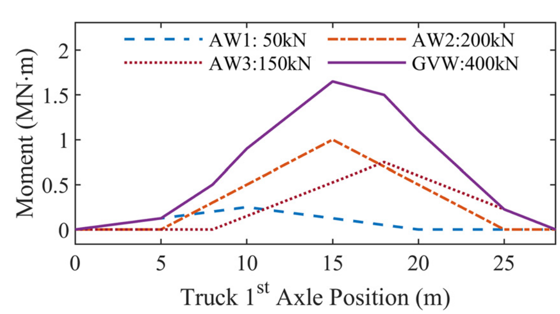

Fig. 2. Bending moments at midspan of the bridge due to the vehicle axle weights and whole-vehicle GVW.

resolution of 0.05 m for the real axle spacing is considered acceptable. Using Moses's algorithm, the weights of the 241 axles were obtained, and they are plotted in Fig. 3. It can be seen in Fig. 3 that the identified weights of most virtual axles are zero, and there are three positive peaks with ordinates of (0, 50.02), (–5, 231.80), and (–8, 173.80), which match the three true axles of the truck. However, it should be noted that the axle weights identified at the end of this step are not yet the final results. Based on the positions of the three peak points, the axle spacings of the truck were determined accurately as 5 and 3 m. To refine the axle weight calculation, one more step is performed. The identified axle positions (0, –5 m, –8 m) were fed into Eq. (3) to form the matrix **I** (this time with only the true axles), and the exact axle weights were found, using Moses's algorithm, to equal the exact values of 50, 200 and 150 kN.

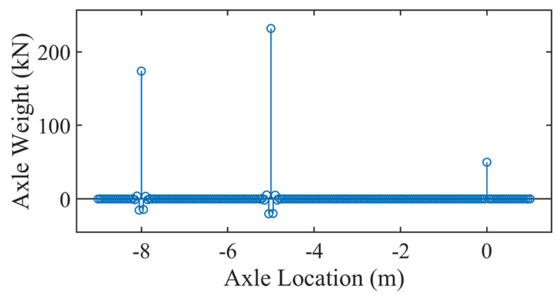

Fig. 3. Identified weights of the virtual axles.

From the example, it can be seen that the proposed method is straightforward and easy to implement, but it may fail if there is significant noise in the original bending strain signals. Fig. 4(a) shows the same example with 2% white noise added to the measured' bending moment. As a result, significant chaos is brought into the identified results, as presented in Fig. 4(b).

To address this problem, constraints were set in the identification process. It is known that vehicle axle weights cannot be negative. Thus, the constraint $P \geq 0$ is set when solving the least-squares problem of Eq. (4), expressed as follows:

$$\text{Minimize } \|\mathbf{M} - \mathbf{I} \cdot \mathbf{P}\|_2^2 \text{ subject to } \mathbf{P} \geq 0 \tag{6}$$

where $\mathbf{0}$ = row vector of zeros with the number of elements equal to the number of virtual axles. The expression in Eq. (6) is a nonnegative least-squares (NNLS) problem, which can be solved using the active set algorithm (Lawson and Hanson 1974). After applying this constraint, only a few virtual axles will be nonzero, as presented in Fig. 4(c). A further constraint is imposed on axle spacing. A reasonable lower limit, which is denoted as AS_{min}, can be considered to be 1.4 m. More closely spaced axles are still possible but will be considered as a single moving weight. By introducing these two constraints, the problem with noisy data can then be effectively solved. The proposed virtual axle method is summarized in Fig. 5, with full details given in the Appendix. The notation is given in Table 1.

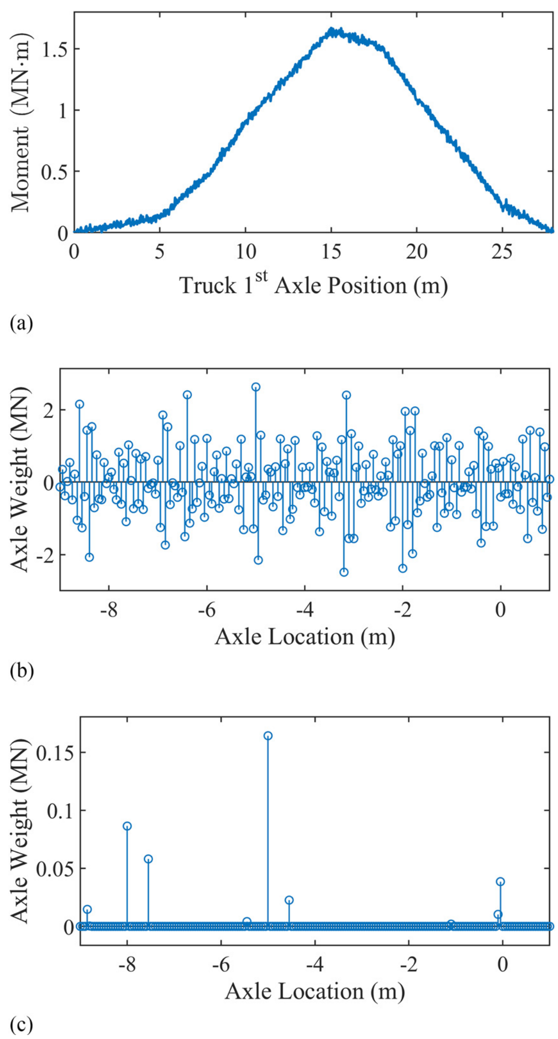

Fig. 4. Numerical example with bridge response polluted with 2% noise: (a) noisy bending moment; (b) identified weights of virtual axles; and (c) results of NNLS.

Numerical Study

Vehicle–Bridge Interaction Model

The problem of vehicle–bridge interaction (VBI) has been studied extensively over the past two decades (Deng et al. 2019). The dynamic equations of the vehicle–bridge system can be established according to the relationship between their displacements and the interactive forces at the tire–bridge-surface contact positions (Deng and Cai 2010), as follows:

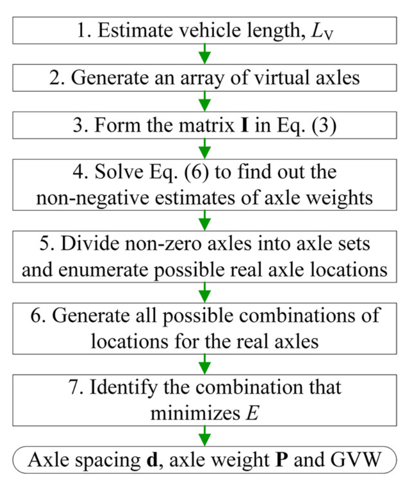

Fig. 5. Summary of VA procedure.

Table 1. Parameters of the VA method

Parameter	Symbol	Description
Input	L_B	Bridge length
	$\mathbf{M}$	Time history of bending moment (or other global bridge response, such as flexural strain or shear strain)
	$I(x)$	Bridge influence line as a function of axle location x
	v	Vehicle speed
	$\mathrm{AS}_{\min}$	Minimum axle spacing
	δ_x	Resolution of axle spacing (real or virtual)
Output	N_A	Number of vehicle axles
	$\mathbf{d}$	Vector of axle spacings
	$\mathbf{P}$	Vector of axle weights
	GVW	Gross vehicle weight

$$\begin{cases} \mathbf{M}_V\ddot{Z} + \mathbf{C}_V\dot{Z} + \mathbf{K}_V Z = \mathbf{N}_V \cdot F_c + G_V \\ \mathbf{M}_B\ddot{Y} + \mathbf{C}_B\dot{Y} + \mathbf{K}_B Y = \mathbf{N}_B \cdot F_c \end{cases} \tag{7}$$

where $\mathbf{M}_V, \mathbf{C}_V, \mathbf{K}_V$ and $\mathbf{M}_B, \mathbf{C}_B, \mathbf{K}_B$ = mass, damping, and stiffness matrices for the vehicle and the bridge, respectively; $\mathbf{N}_V$ and $\mathbf{N}_B$ = shape functions of the vehicles and the bridge, respectively; Z and Y = displacement vectors of vehicles and the bridge, respectively; and $\mathbf{G}_V$ = vector of vehicle gravity forces. The vector $\mathbf{F}_c = \{f_1, f_2, \ldots, f_{2N_A}\}^T$ contains the contact forces between the vehicle tires and the bridge surface, the components of which are given by

$$f_i = k_i[z_i(t) - y_i(t) - r_i(t)] + c\left[\dot{z}_i(t) - \dot{y}_i(t) - \dot{r}_i(t)\right] \tag{8}$$

where $z_i(t)$, $y_i(t)$, and $r_i(t)$ = displacements of the vehicle tires, the bridge in the vertical direction, and the bridge-surface roughness at the contact points at time t, respectively.

Several numerical integration methods can be used to solve Eq. (8). Modal superposition was used in this study to improve the computational efficiency (Deng et al. 2018c). A MATLAB program was developed based on the iterative Newmark-β algorithm to solve the equation in the time domain. The details of the numerical algorithm and validation of the computing program have been given by Deng and Cai (2010) and He et al. (2016). The flexural strains of the bridge were then obtained according to the strain-displacement relationship once the displacement of the bridge was determined.

Simulation Setup

In this study, a 20-m-span simply-supported girder bridge with four T-beams and two truck models, consisting of a two-axle truck and a three-axle truck, were adopted in the numerical simulation. The two-axle truck has a gross vehicle weight (GVW) of 73.5 kN, and the three-axle truck has a GVW of 320.1 kN. The bridge and truck models are illustrated in Fig. 6. The details can be found in He et al. (2016). In the numerical simulation, two levels of road-surface condition (RSC), smooth and coarse, were considered. A Class A level road profile, according to ISO-8608 (ISO 1995), which has been commonly adopted in numerical simulations, was adopted for the coarse RSC. The trucks were set to travel along the center of the left lane, as presented in Fig. 6(a), at different speeds ranging from 10 to 30 m/s in intervals of 5 m/s. For each loading scenario under the coarse RSC, 10 random road-surface profiles were generated. The truck was then set to run 10 times independently, and the average value of the identified axle spacing, axle weight, and GVW of the 10 trials, as well as their standard deviations, were used in the later error analysis.

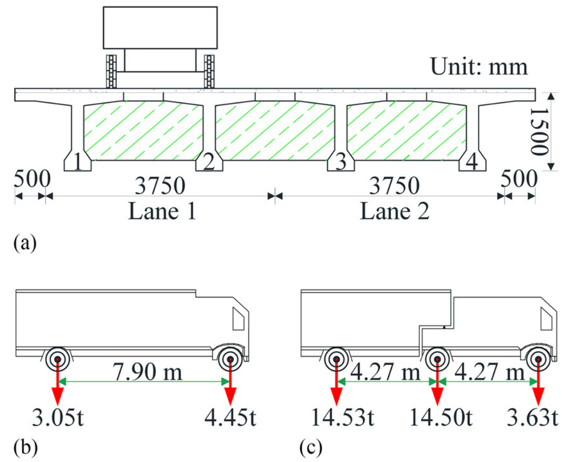

Fig. 6. Bridge and trucks considered: (a) bridge cross section and vehicle loading position; (b) two-axle truck; and (c) three-axle truck.

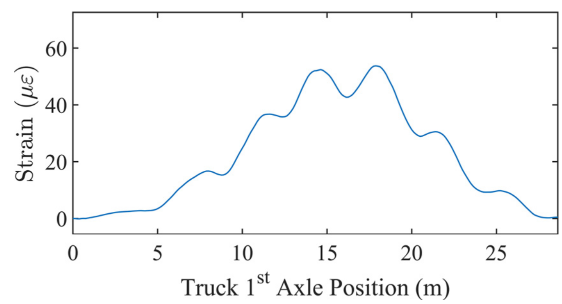

Fig. 7. Time history of bending strain of Girder 2 at midspan (three-axle truck, 25 m/s, coarse road surface).

VBI Simulation

A simple example using the three-axle truck is used to demonstrate the proposed method in detail. Fig. 7 presents the flexural strain measured on the underside of the second girder at the midspan. In this case, the truck was set to run at a speed of 25 m/s. Fig. 8(a) presents the interim results when the fourth step (the finding of nonnegative estimates in Fig. 5) is complete, setting the resolution of axle spacing to δ_x = 0.05 m and the minimum axle spacing to $\mathrm{AS}_{\min}$ = 1.4 m. As a result of this step, eight axle locations $\hat{\mathbf{x}}$ = {−8.350, −8.250, −4.400, −4.350, −0.650, −0.350, 0.500, 0.600} corresponding to VAs with nonzero weights were found. With the limitation set on $\mathrm{AS}_{\min}$, these axles were then divided into three sets: {−8.350, −8.250}, {−4.400, −4.350}, {−0.650, −0.350, 0.500, 0.600}. Each of the three axle sets was expected to contain one true axle within its boundaries. Theoretically, the true axle may be located at any position within the boundary of each axle set. Next, by adopting the same resolution of δ_x for axle location as used previously for axle spacing, all possible locations of each true axle were considered, as presented in Fig. 8(b). Then, all combinations of possible locations of the three real axles were found following Step 6. Finally, the norm of the residual corresponding to each combination of possible axle locations was calculated, and the axle locations and weights corresponding to the global minimum, for all combinations, was adopted (Step 7).

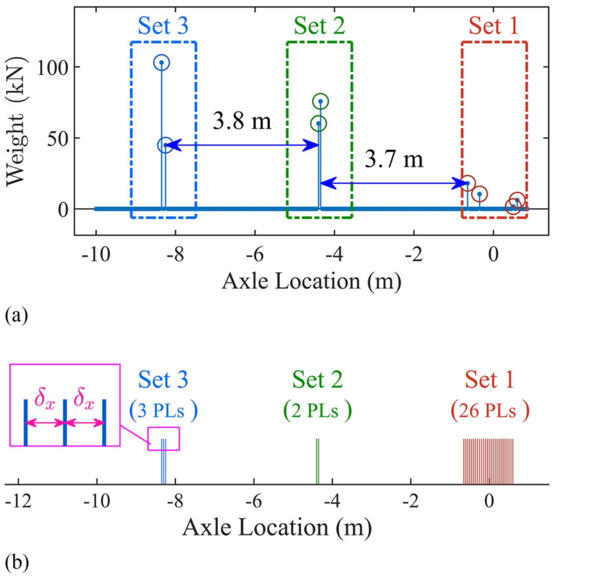

Fig. 8. (a) First solution of the NNLS problem; and (b) possible locations of each true axle (PL = possible location).

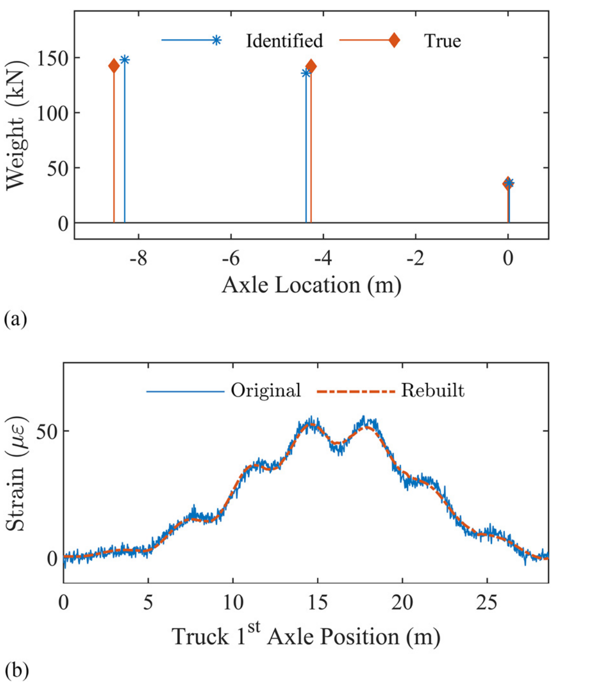

Fig. 9. Results of VA algorithm (three-axle truck, 25 m/s, coarse road surface): (a) identified axle locations and weights; and (b) original and rebuilt strain response of Girder 2 at midspan.

Table 2. Relative error of identification results

Method	Relative error (%) AW$_1$	AW$_2$	AW$_3$	GVW
VA method	2.28	−4.45	3.82	−0.02
Moses's algorithm	−19.16	5.80	−0.41	0.27

Note: AW = axle weight.

The identified results using the proposed VA method are plotted in Fig. 9(a). It can be seen that the axle spacing and weights were successfully identified by the proposed VA method. The bridge strain obtained from numerical simulation and that rebuilt based on the results of the VA process are plotted in Fig. 9(b). It should be noted that to be more realistic, 5% white noise was added into the measured strain before feeding it into the VA procedure. As presented in Fig. 9(b), the rebuilt signal based on the identified results is reasonably close to the original. To compare the effectiveness of the proposed VA method, Moses's algorithm was also used to identify the axle weight and GVW. The results identified by the VA method and those identified by the original Moses's algorithm are listed in Table 2. It should be noted that both vehicle speed and axle spacings were assumed as known inputs by Moses's algorithm, whereas only vehicle speed was assumed as a known input in the proposed method. From Table 2, it can be seen that, for the case considered, the proposed VA method was able to achieve a similar level of accuracy or even better in some cases.

Fig. 10 presents the VA identification results of axle location, weight, and GVW for all the cases considered. From Fig. 10, it can be seen that the spacings and weights for both the two-axle and the three-axle trucks can be successfully obtained by the proposed VA method. Table 3 summarizes the mean value ($\bar{x}$) and standard

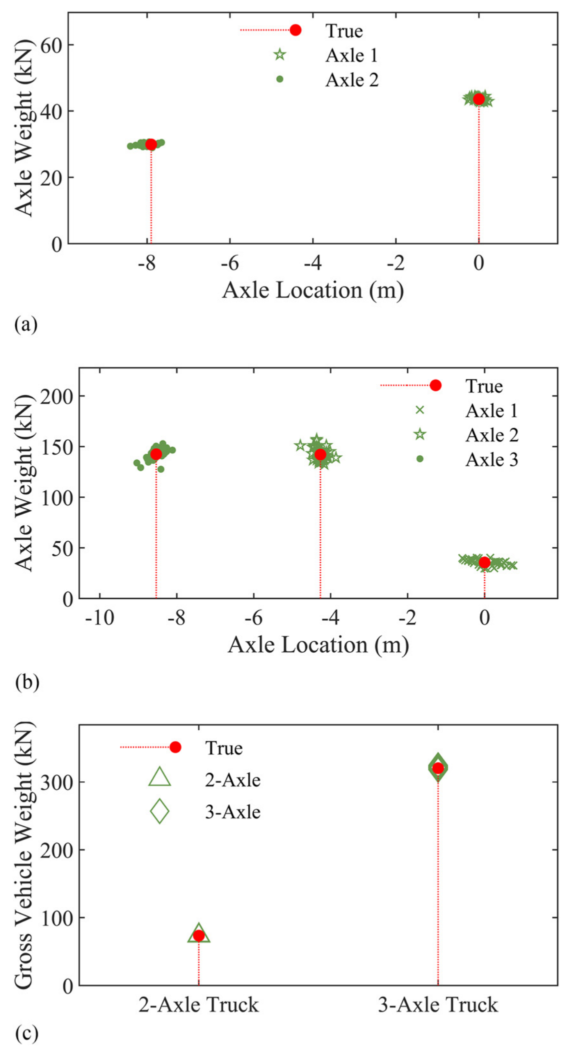

Fig. 10. Identified axle positions, axle weights, and GVW: (a) two-axle truck; (b) three-axle truck; and (c) GVW.

J. Bridge Eng., 2019, 24(9): 04019086

deviation (s) of the percentage of relative errors of the identified axle spacings. The mean identification errors of axle spacing for both trucks can be seen to be under 5%.

The corresponding results for axle weights and GVWs are presented in Table 4. It can be seen that the VA relative errors, for both axle and gross weights, are all under 1% and are less than those of Moses's algorithm in most cases. It should be noted that accuracy in numerical simulations is generally much greater than in field tests. The significance of these results is, therefore, a relative one (i.e., achieving comparable performance to Moses's algorithm with exact axle spacings, without the use of axle detectors).

The standard deviations of the relative errors for both trucks are significant, and the VA method performs less well than Moses's algorithm using exact (true) axle spacings. It is of note that one axle of the three-axle truck is much lighter than the other two, which is a particular challenge in the presence of dynamics. In general, the identification results for heavier axles have better accuracy than those for lighter axles.

Figs. 11 and 12 present the relative identification errors for the axle spacing, axle weights, and gross weights of the two-axle truck traveling at various vehicle speeds under smooth and coarse RSCs. For the results with the coarse road surface, as presented in Fig. 12, the error bars indicate the 90% confidence intervals of the results from 10 runs with randomly generated Class A level road-surface profiles.

From Figs. 11 and 12, it can be seen that the axle spacings, axle weights, and gross weights of the two-axle truck were consistently identified by the VA method. The mean relative errors of the identified results are all below 2%. Unsurprisingly, the identification error increase when road roughness is introduced. The errors also tend to increase with increased vehicle speed but are generally below 4% with 90% confidence.

The corresponding results for the three-axle truck are given in Figs. 13 and 14. In this case, the mean values of relative error are generally less than 5%, and the accuracy error is less than 9% with 90% confidence. However, both the mean relative errors and the confidence intervals of the results for the three-axle truck are larger than those for the two-axle truck. This may be influenced by the relatively big difference between the weights of three axles of the three-axle truck. As is usual for BWIM, the GVW accuracies are generally better. The phenomenon of high identification accuracy on GVW and relatively low accuracy on axle weight has been reported in many other studies and can be attributed to many factors, such as the low sensitivity of the bridge response to each individual axle of multiaxle trucks and the effect of noise (González et al. 2012; Zhao et al. 2014). The effects of RSC on the identification errors show similar patterns to those observed for the two-axle truck.

The results did not show a convincing pattern for the effect of vehicle speed on the identification accuracy. Peaks of errors occur at various speeds for different axles and trucks. These errors are higher for some particular speeds (e.g., 25 m/s for axle weight errors of two-axle truck and 30 m/s for spacing errors of three-axle truck). This could be a resonance effect, where the vehicle's bounce frequency or the pseudo-frequency associated with vehicle speed/axle spacing is resonating with the bridge's first natural frequency.

Table 3. Mean ($\bar{x}$) and standard deviation (s) of relative error of identified axle spacing

Truck	Relative error (%) AS$_1$ $\bar{x}$	AS$_1$ s	AS$_2$ $\bar{x}$	AS$_2$ s
Two-axle truck	−1.1	1.6	—	—
Three-axle truck	0.5	4.0	4.3	6.1

Note: AS = axle spacing.

Experimental Validation

Experiment Setup

To investigate the accuracy and effectiveness of the proposed VA method, scaled VBI model tests were carried out in the laboratory.

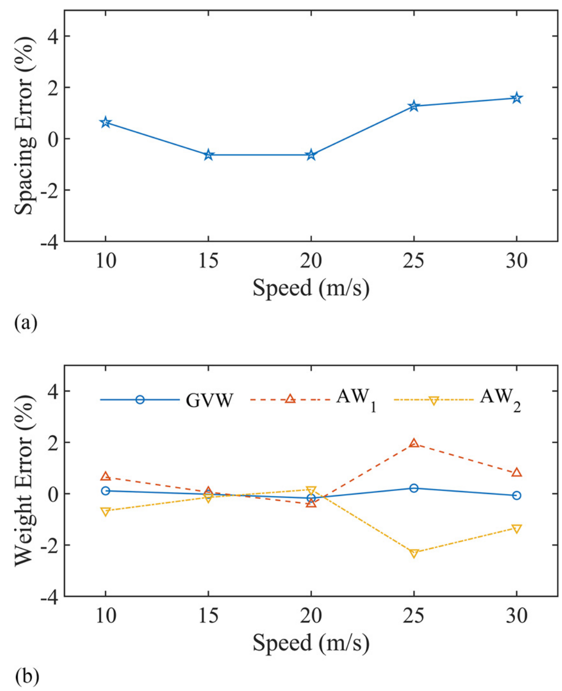

Fig. 11. Identification error (two-axle truck, smooth road surface): (a) axle spacing; and (b) weight.

Table 4. Mean ($\bar{x}$) and standard deviation (s) of relative error of identified weight results

Truck	Method	Relative error (%) AW$_1$ $\bar{x}$	AW$_1$ s	AW$_2$ $\bar{x}$	AW$_2$ s	AW$_3$ $\bar{x}$	AW$_3$ s	GVW $\bar{x}$	GVW s
Two-axle truck	VA method	0.5	1.7	−0.6	2.4	—	—	0.1	0.3
	Moses's algorithm	1.0	1.2	−0.7	1.5	—	—	0.3	0.5
Three-axle truck	VA method	−0.5	7.0	0.2	3.8	0.6	3.9	0.3	0.5
	Moses's algorithm	1.9	5.4	−0.9	2.7	0.3	2.1	−0.1	0.4

Note: AW = axle weight.

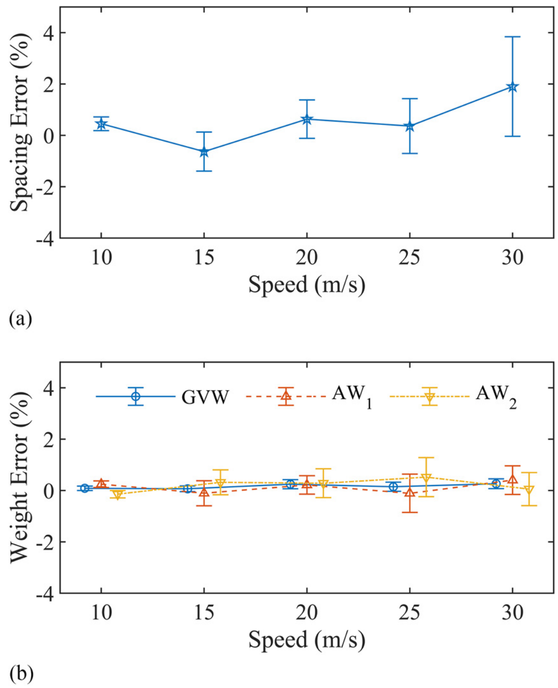

Fig. 12. Identification error (two-axle truck, coarse road surface): (a) axle spacing; and (b) weight.

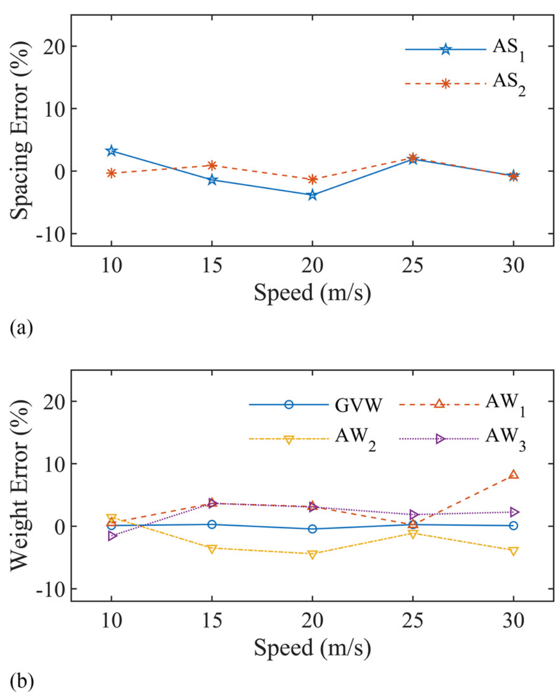

Fig. 13. Relative errors of identification results (three-axle truck, smooth road surface): (a) axle spacing; and (b) weight.

The tests were conducted on a dedicated VBI test platform, as illustrated in Fig. 15(a).

The scaled bridge model, presented in Fig. 15(b), was designed according to the similarity principle, and the prototype is the bridge model adopted in the numerical simulation section. The scale ratios of length and strain were 1:0.119 and 1:1, respectively. Polymethyl methacrylate (PMMA) material was adopted as the material for the

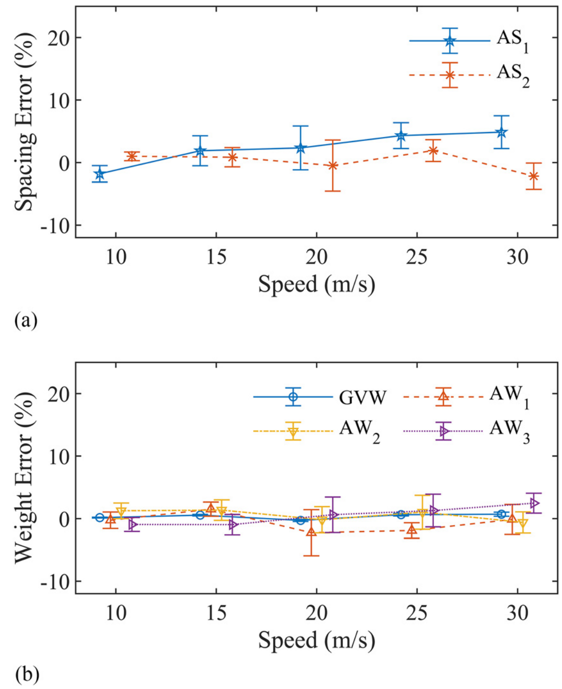

Fig. 14. Relative errors of identification results (three-axle truck, coarse road surface): (a) axle spacing; and (b) weight.

scaled bridge model. The steel test truck model, presented in Fig. 15(c), was also designed according to similarity principles with the same scale ratio. The axle spacing and axle weights of the model truck axles are marked in Fig. 15(c). The gross weights of the scaled truck model and the prototype truck were 281 N and 245 kN, respectively. Aside from the bridge and truck models, the VBI test platform also contained an acceleration ramp, a cushion for deceleration, and a T-shaped guide rail for direction control.

In this study, two polyvinylidene fuoride (PVDF) cables were placed on the top surface of the bridge model, as presented in Fig. 15, to identify vehicle speed. The identified speed was then fed into the VA method as the true speed. In addition, a foil strain gauge was installed underneath the G2 girder at the midspan to serve as weighing sensor. More details of the test platform and experimental setup can be found in He et al. (2016).

Calculating Influence Line from Test Data

The influence line (IL) of bending strain can be extracted from the bridge response by setting the truck to pass over the bridge at a low speed (OBrien et al. 2006). To reduce the variation caused by a single event, the truck model was set to run multiple times at low speeds of approximately 1 m/s (González et al. 2012). The ILs of bending strain of the G2 girder were then extracted from the measured strains of the test runs, for the cases of both the truck running along the left lane and the truck running along the right lane. Before calculating the Il, a moving average filter provided by MATLAB was used to remove the random noise contained in the measured strain signal. In the filtered signal, each data point was calculated using 3% of the total number of the neighbored data points. Finally, the many ILs were averaged to get the final IL to be used in the following identification procedure. For the purpose of illustration, Fig. 16 presents three ILs for the G2 girder estimated using OBrien's method (OBrien et al. 2006) and the final IL adopted based on the average of seven ILs when the truck was in the left lane.

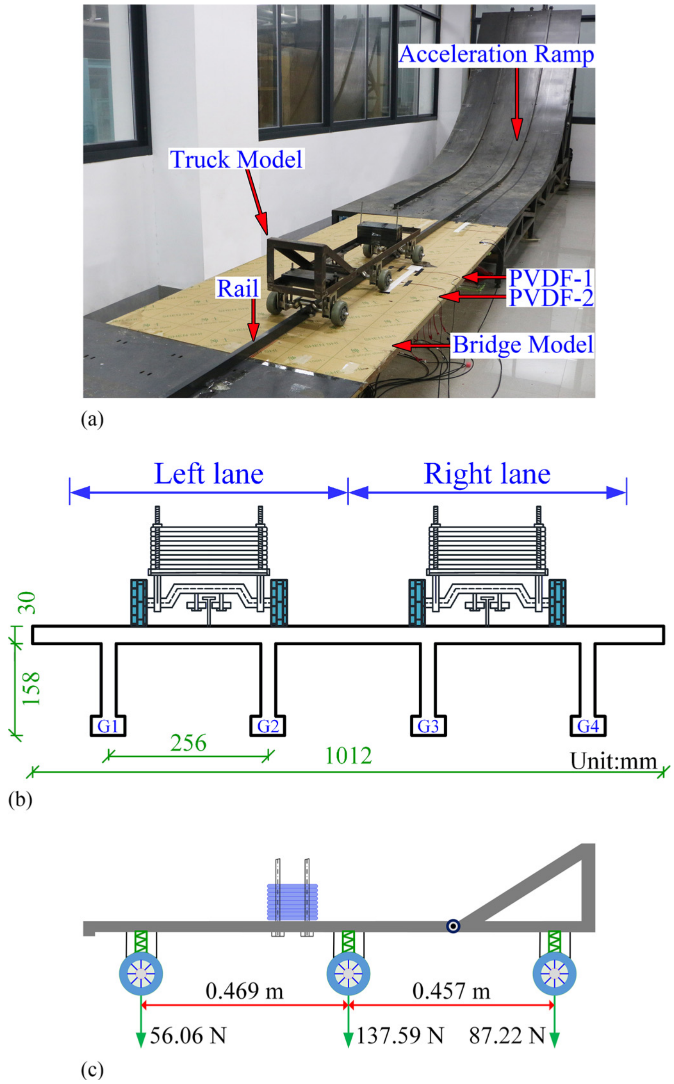

Fig. 15. (a) Test platform; (b) bridge section and loading positions; and (c) truck model.

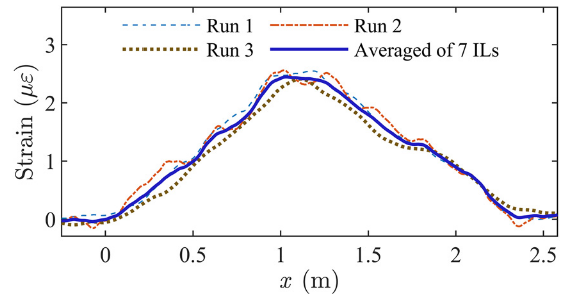

Fig. 16. Strain IL for the midspan of Girder 2 (vehicle in left lane).

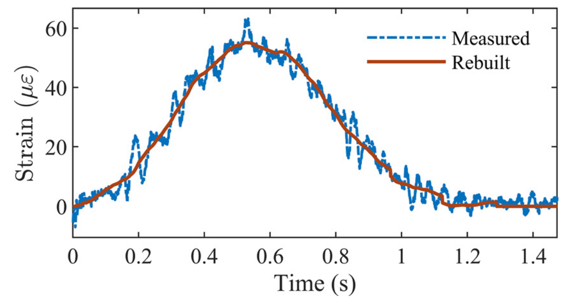

Fig. 17. Typical measured and rebuilt strain of Girder 2 (left lane, v = 2.85 m/s).

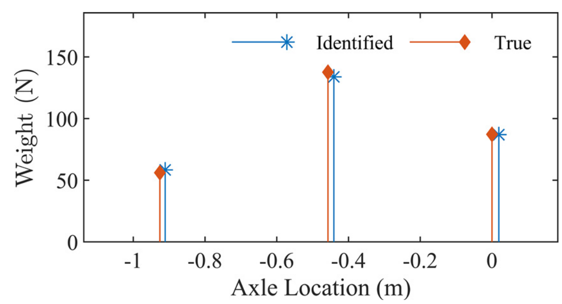

Fig. 18. Identification results by the VA method (left lane, $v = 2.85$ m/s).

It should be noted that to obtain the bridge ILs, the axle spacings of the calibration truck need to be measured beforehand by using external devices.

Results of Experiment

In the experiments, the truck model was set to run along both the left and the right lanes. The actual speed of the model truck ranged from 1 to 5 m/s, corresponding to 10.4 to 52 km/h of the truck prototype.

Fig. 17 presents a typical time-history curve of the bridge strain measured at the midspan of the G2 girder under a vehicle speed of 2.85 m/s. From Fig. 17, it can be seen that a notable dynamic effect exists in the measured strain signal. By feeding this intact signal into the identification procedure of the VA method, the axle locations and weights were first obtained, and the axle spacing and GVW were then calculated. It should be noted that in the identification procedure, the minimum axle spacing and the spacing of VAs were determined as $\mathrm{AS}_{\min} = 1.4\,\mathrm{m} \times 0.119 = 0.167\,\mathrm{m}$ and $\delta_x = 0.05\,\mathrm{m} \times 0.119 = 0.006\,\mathrm{m}$, based on the similarity principle.

Fig. 18 presents the identification results of axle location and weights by the VA method. The strain rebuilt based on the measured IL and the identified axle information are plotted in Fig. 17. It is seen that the VA method can successfully identify the axle information, including both the spacing and the weights, of the moving vehicle, even under noisy conditions.

Table 5 summarizes the relative identification errors by the proposed VA method for the cases with the truck traveling along both the left and right lanes. The strain from Girder 2 was used in all the cases investigated. The vehicle speeds were predicted from the signals of the PVDF cables and were considered to be true vehicle speeds in testing the accuracy of the VA method. From Table 5, it can be seen that the identification errors of the axle spacing and GVW using the proposed VA method are all within 5%, and the errors of axle weight are less than 7.6%, regardless of the vehicle speed and its lateral position.

For the purpose of comparison, the relative errors of axle spacing using the PVDF cables and the relative errors of axle weight and GVW predicted using Moses's algorithm are also listed in Table 5. It can be seen that good accuracy was achieved on axle spacing identification by both the VA method and the PVDF signals, with

Table 5. Relative errors of identification results

Loading position	Speed (m/s)	Relative error (%) PVDF AS_1	AS_2	Moses's algorithm AW_1	AW_2	AW_3	GVW	VA method AS_1	AS_2	AW_1	AW_2	AW_3	GVW
Left lane	1.05	−0.74	0.24	7.61	−6.01	−1.19	−0.82	−0.30	−0.74	1.33	−1.28	−1.30	−0.77
	1.96	−1.67	1.08	8.57	−7.17	−4.00	−1.65	−0.20	1.08	7.53	−2.31	−2.99	−0.56
	2.87	1.68	−0.01	0.73	−1.61	3.04	0.05	−1.07	0.86	0.33	−1.30	1.14	−0.22
	3.71	1.11	1.24	8.26	−12.46	13.87	−0.77	−2.65	−1.43	−0.14	1.00	−5.16	−1.14
	4.82	0.63	0.78	2.20	−2.75	−0.82	−0.83	−0.44	0.24	−0.27	−3.91	−5.25	−3.60
Right lane	1.01	−0.32	−1.43	−2.21	1.60	−2.18	−0.33	2.40	−0.35	−0.42	0.65	−1.11	−0.11
	1.90	0.59	0.59	12.73	−12.12	9.38	−0.12	0.26	0.98	5.92	−4.08	1.98	−0.20
	2.91	−0.92	0.72	4.99	−5.19	1.19	−0.76	−0.89	−0.39	1.63	−1.30	−2.16	−0.98
	3.69	−0.83	0.72	2.26	−2.19	−1.38	−0.64	−0.08	1.18	3.54	−1.52	−0.72	−0.27
	4.65	0.91	0.96	−1.31	0.08	1.20	−0.13	−0.11	0.81	1.64	−1.13	1.12	0.12
Mean value	—	0.04	0.49	4.38	−4.78	1.91	−0.60	−0.31	0.23	2.11	−1.52	−1.45	−0.77
Standard deviation	—	1.08	0.77	4.85	4.78	5.59	0.50	1.26	0.90	2.74	1.64	2.51	1.07

Note: The speed is identified from the PVDF signals. AS = axle spacing; and AW = axle weight.

all errors below 2.65% and 1.68%, respectively. Also, most relative errors of the GVW are under 2% for the VA method and Moses's algorithm, except that the error for one case by the VA method reaches 3.6%. From these results, it seems that the accuracy on gross weight identification by the VA method was slightly worse than that for Moses's algorithm. However, the VA method achieved better accuracy in axle weight identification than Moses's algorithm in that the mean errors and standard deviations for the VA method were all less than those for Moses's algorithm.

Summary and Conclusions

In this study, a novel bridge weigh-in-motion algorithm (i.e., the VA method) is proposed to identify the number of axles, axle spacings, axle weights, and gross weights of vehicles passing over highway bridges. The proposed VA method uses only the global bending strain of bridge girders to detect the axle spacings and axle weights of moving vehicles, providing an effective and efficient alternative for the next generation of NOR BWIM systems. Numerical simulations and laboratory experiments were performed to investigate the performance of the proposed VA method. The effects of vehicle speed, vehicle lateral position, and bridge-surface condition on the identification accuracy were investigated. Based on the results of this study, it is found that once vehicle speed is known, the two main goals of a BWIM system, namely, axle detection and weight prediction, can be accomplished by the proposed method using only one weighing sensor. Acceptable identification accuracy has also been achieved for a range of vehicle speeds, lateral positions, and RSCs.

Conventional NOR BWIM systems usually require additional FAD sensors for axle detection to achieve weight prediction using strain sensors. In contrast, the proposed VA method obtains axle information directly from the global bending strain of the bridge through only weighing sensors. Furthermore, it sets no restriction on the type of bridge or the type of bridge response, as long as the IL function can be obtained. These advantages make the proposed VA method an effective alternative for commercial NOR BWIM systems.

The conclusions in this study were made based on single truck scenarios through numerical simulation and scaled model testing. Further research could be conducted to investigate the scenarios with multiple trucks and to evaluate the performance of the VA method in the field.

Appendix. Details of VA Procedure

Step	Procedure
1	Estimate the length of the vehicle as $L_V = T \cdot v - L_B$, where T is the time duration for the vehicle to cross the bridge, which may be roughly estimated from the time history of bridge responses. Otherwise, L_V can be assigned a reasonably large value based on engineering judgment.
2	Assume that the vehicle has virtual axles distributed evenly with spacing of δ_x, and define the locations of the virtual axles as $\mathbf{x} = \{x_1, x_1 - \delta_x, x_1 - 2\delta_x, \ldots, x_1 - N_0 \cdot \delta_x\}$, where $N_0 = \lceil L_V/\delta_x \rceil$, in which $\lceil x \rceil$ is a ceiling function that returns the smallest integer that is no less than x, and x_1 is the location of the first virtual axle.
3	Form the matrix $\mathbf{I}$ shown in Eq. (3).
4	Solve the NNLS problem [i.e., Eq. (6)] by using the active set algorithm [function *lsqnonneg* provided by MATLAB (Mathworks 2018)] to obtain the first estimate of the virtual axle weight vector, $\widehat{\mathbf{P}} = \{\widehat{P}_i \mid \widehat{P}_i > 0\}$; the associated axle locations, $\widehat{\mathbf{x}} = \{x_i \mid \widehat{P}_i > 0\}$; and the spacings $\widehat{\mathbf{d}}$ between the axles with positive weights.
5	Divide the vector $\widehat{\mathbf{x}}$ into sets according to the following condition: those adjacent virtual axles with spacing less than AS_{min} belong to the same virtual axle set. Then, refill each of these sets, within its range, with evenly spaced virtual axles and denote them as vectors $\mathbf{g}_1, \mathbf{g}_2, \ldots, \mathbf{g}_{N_A}$.
6	Create all possible combinations of vectors $\{\mathbf{g}_1, \mathbf{g}_2, \ldots, \mathbf{g}_{N_A}\}$ and denote them as $\{\mathbf{X}^1, \mathbf{X}^2, \ldots, \mathbf{X}^{N_c}\}$, where each combination $\mathbf{X}^l$ is considered as a possible candidate for the locations of the N_A axles, and $N_c = \prod_{i=1}^{N_A} \mathrm{Numel}(\mathbf{g}_i)$ is the total number of all possible combinations, in which $\mathrm{Numel}(\mathbf{g})$ returns the number of elements of the vector $\mathbf{g}$.
7	For each possible candidate, $\mathbf{X}^l$, calculate the axle weights $\mathbf{P}^l$ and the Euclidean norm E^l expressed in Eq. (4) by using Moses's algorithm. Find out the index $\widehat{l}$ of the smallest element of the set, $\mathbf{E} = \{E^1, E^2, \ldots, E^{N_c}\}$. The axle spacing, axle weights, and GVW can then be obtained as $\mathbf{d} = \mathrm{Diff}(\mathbf{X}^{\widehat{l}})$, $\mathbf{P} = \mathbf{P}^{\widehat{l}}$, $\mathrm{GVW} = \sum_{j=1}^{N_A} P_j^{\widehat{l}}$, where $\mathrm{Diff}(\mathbf{X})$ returns the differences between adjacent elements of the vector $\mathbf{X}$.

Acknowledgments

The authors acknowledge the financial support provided by the National Natural Science Foundation of China (51778222) and the Key Research Project of Hunan Province (2017SK2224).

References

Bao, T., S. K. Babanajad, T. Taylor, and F. Ansari. 2016. "Generalized method and monitoring technique for shear-strain-based bridge weigh-in-motion." *J. Bridge Eng.* 21 (1): 4015029. https://doi.org/10.1061/(ASCE)BE.1943-5592.0000782.

Deng, L., T. Bi, W. He, and W. Wang. 2017. "Vehicle weight limit analysis method for reinforced concrete bridges based on fatigue life." [In Chinese.] *China J. Highw. Transp.* 30 (4): 72–78.

Deng, L., and C. S. Cai. 2010. "Development of dynamic impact factor for performance evaluation of existing multi-girder concrete bridges." *Eng. Struct.* 32 (1): 21–31. https://doi.org/10.1016/j.engstruct.2009.08.013.

Deng, L., L. Duan, W. He, and W. Ji. 2018a. "Study on vehicle model for vehicle-bridge coupling vibration of highway bridges in China." [In Chinese.] *China J. Highw. Transp.* 31 (7): 93–100.

Deng, L., W. He, Y. Yu, and C. S. Cai. 2018b. "Equivalent shear force method for detecting the speed and axles of moving vehicles on bridges." *J. Bridge Eng.* 23 (8): 4018057. https://doi.org/10.1061/(ASCE)BE.1943-5592.0001278.

Deng, L., W. He, Y. Yu, and W. Wang. 2018c. "Research progress in theory and applications of highway vehicle-bridge coupling vibration." [In Chinese.] *China J. Highw. Transp.* 31 (7): 38–54.

Deng, L., W. Yan, and L. Nie. 2019. "A simple corrosion fatigue design method for bridges considering the coupled corrosion-overloading effect." *Eng. Struct.* 178: 309–317. https://doi.org/10.1016/j.engstruct.2018.10.028.

González, A., J. Dowling, E. J. OBrien, and A. Žnidarič. 2012. "Testing of a bridge weigh-in-motion algorithm utilising multiple longitudinal sensor locations." *J. Test. Eval.* 40 (6): 104576. https://doi.org/10.1520/JTE104576.

He, W., L. Deng, H. Shi, C. S. Cai, and Y. Yu. 2016. "Novel virtual simply supported beam method for detecting the speed and axles of moving vehicles on bridges." *J. Bridge Eng.* 22 (4): 4016141.

Ieng, S. S., A. Zermane, F. Schmidt, and B. Jacob. (2012). "Analysis of B-WIM signals acquired in Millau orthotropic viaduct using statistical classification." In *Proc., 6th Int. Conf. on Weigh-in-Motion (ICWIM 6)*, edited by B. Jacob, A.-M. McDonnell, F. Schmidt, and W. Cunagin, 43–52. Hoboken, NJ: Wiley.

ISO. 1995. *Mechanical Vibration-Road Surface Profiles-Reporting of Measured Data*. ISO-8608. Geneva: ISO.

Jacob, B. 2010. "Improving truck safety: Potential of weigh-in-motion technology." *IATSS Res.* 34 (1): 9–15. https://doi.org/10.1016/j.iatssr.2010.06.003.

Kalhori, H., M. M. Alamdari, X. Zhu, B. Samali, and S. Mustapha. 2017. "Non-intrusive schemes for speed and axle identification in bridge-weigh-in-motion systems." *Meas. Sci. Technol.* 28 (2): 25102. https://doi.org/10.1088/1361-6501/aa52ec.

Kalin, J. 2006. "Practical implementation of nothing-on-the-road bridge weigh-in-motion system." In *Proc., 9th Int. Symp. on Heavy Vehicle Weights and Dimensions*. Ottawa: Transportation Association of Canada.

Lawson, C. L., and R. J. Hanson. 1974. *Solving least-squares problems.* Upper Saddle River, NJ: Prentice Hall.

Lydon, M., D. Robinson, S. E. Taylor, G. Amato, E. J. OBrien, and N. Uddin. 2017. "Improved axle detection for bridge weigh-in-motion systems using fiber optic sensors." *J. Civ. Struct. Health Monit.* 7 (3): 325–332. https://doi.org/10.1007/s13349-017-0229-4.

Lydon, M., S. E. Taylor, D. Robinson, A. Mufti, and E. J. OBrien. 2016. "Recent developments in bridge weigh in motion (B-WIM)." *J. Civ. Struct. Health Monit.* 6 (1): 69–81. https://doi.org/10.1007/s13349-015-0119-6.

Mathworks. 2018. "lsqnonneg" Accessed October 20, 2018. https://www.mathworks.com/help/releases/R2018a/matlab/ref/lsqnonneg.html.

Moses, F. 1979. "Weigh-in-motion system using instrumented bridges." *Transp. Engrg. J.* 105 (3): 233–249.

OBrien, E., D. Hajializadeh, N. Uddin, D. Robinson, and R. Opitz. 2012. "Strategies for axle detection in bridge weigh-in-motion systems." In *Proc., Int. Conf. on Weigh-in-Motion (ICWIM 6)*, edited by B. Jacob, A.-M. McDonnell, F. Schmidt, and W. Cunagin, 79–88. Hoboken, NJ: Wiley.

OBrien, E. J., M. Quilligan, and R. Karoumi. 2006. "Calculating an influence line from direct measurements." *Proc. Inst. Civ. Eng. Bridge Eng.* 159 (1): 31–34. https://doi.org/10.1680/bren.2006.159.1.31.

OBrien, E. J., and A. Žnidarič, eds. 2001. *Weighing-in-motion of axles and vehicles for Europe (WAVE)*. Rep. of Work Package 1.2. Slovenia: Bridge WIM Systems, Zavod za gradbenistvo (ZAG).

Ojio, T., C. H. Carey, E. J. OBrien, C. Doherty, and S. E. Taylor. 2016. "Contactless bridge weigh-in-motion." *J. Bridge Eng.* 21 (7). https://doi.org/10.1061/(ASCE)BE.1943-5592.0000776.

Quilligan, M., R. Karoumi, and E. J. OBrien. 2002. "Development and testing of a 2-dimensional multi-vehicle bridge-WIM algorithm." In *Proc., 3rd Int. Conf. on Weigh-in-Motion*, edited by B. Jacob, B. McCall, and E. OBrien, 199–208. Dübendorf, Switzerland: International Society for Weigh-In-Motion.

Richardson, J., S. Jones, A. Brown, E. J. OBrien, and D. Hajializadeh. 2014. "On the use of bridge weigh-in-motion for overweight truck enforcement." *Int. J. Heavy Vehicle Syst.* 21 (2): 83–104. https://doi.org/10.1504/IJHVS.2014.061632.

Sekiya, H., K. Kubota, and C. Miki. 2018. "Simplified portable bridge weigh-in-motion system using accelerometers." *J. Bridge Eng.* 23 (1): 04017124. https://doi.org/10.1061/(ASCE)BE.1943-5592.0001174.

Wall, C. J., R. E. Christenson, A. M. H. McDonnell, and A. Jamalipour. 2009. *A non-intrusive bridge weigh-in-motion system for a single span steel girder bridge using only strain measurements*. Rep. No. CT-2251-3-09-5. Rocky Hill, CT: Connecticut Dept. of Transportation.

Yu, Y., C. S. Cai, and L. Deng. 2015. "Vehicle axle identification using wavelet analysis of bridge global responses." *J. Vib. Control* 95 (11): 523–526.

Yu, Y., C. S. Cai, and L. Deng. 2016. "State-of-the-art review on bridge weigh-in-motion technology." *Adv. Struct. Eng.* 19 (9): 1514–1530. https://doi.org/10.1177/1369433216655922.

Yu, Y., C. S. Cai, and L. Deng. 2018. "Nothing-on-road bridge weigh-in-motion considering the transverse position of the vehicle." *Struct. Infrastruct. Eng.* 14 (8): 1108–1122. https://doi.org/10.1080/15732479.2017.1401095.

Zhao, H., N. Uddin, E. J. OBrien, X. Shao, and P. Zhu. 2014. "Identification of vehicular axle weights with a bridge weigh-in-motion system considering transverse distribution of wheel loads." *J. Bridge Eng.* 19 (3): 4013008. https://doi.org/10.1061/(ASCE)BE.1943-5592.0000533.